Iron–Manganese Nodules in Udepts: The Dependence of the Accumulation of Trace Elements on Nodule Size

Yana O. Timofeeva*
Inst. of Biology and Soil Science
Far Eastern Branch of Russian Academy of Sciences
Vladivostok 690022
Russia

Alexander A. Karabtsov
Far Eastern Geological Inst.
Far Eastern Branch of Russian Academy of Sciences
Vladivostok 690022
Russia

Victoria A. Semal'
Inst. of Biology and Soil Science
Far Eastern Branch of Russian Academy of Sciences
Vladivostok 690022
Russia

Far Eastern Federal Univ.
Vladivostok 690950
Russia

Maxim L. Burdukovskii
IInst. of Biology and Soil Science
Far Eastern Branch of Russian Academy of Sciences
Vladivostok 690022
Russia

NataliaV. Bondarchuk
Far Eastern Geological Inst.
Far Eastern Branch of Russian Academy of Sciences
Vladivostok 690022
Russia

Despite extensive studies, little is known about how the properties of Fe-Mn nodules vary according to their size. In this work, we collected nodules from pollution-free Udepts on the west coast of the Pacific Ocean (south Russian Far-East) and studied them using energy dispersive X-ray fluorescence spectroscopy, X-ray diffraction analysis, atomic absorption spectrometry, electron probe microanalysis, and field-emission scanning electron microscopy. The nodules consisted of a complex Mn-Fe-oxide matrix, soil mineral grains, and C-rich areas. The levels of trace element accumulation, morphological features, and chemical and mineralogical compositions of the nodules varied significantly with the size of the nodules. In the small 1- to 2-mm nodules, Co was associated with Mn whereas Zn and Pb were associated with Fe. In the 2- to 3-mm nodules, manganese was the most important determinant for the accumulation of Co, Ni, and Pb. In the large 3- to 5-mm nodules, Co, Ni, Cu, Zn, and Pb were predominantly associated with Fe. Additionally, in the large nodules, the association of Mn with trace elements was less prominent compared to Fe. The main peculiarities of the medium and large nodules were (i) the presence of primary Mn-Fe-containing minerals in the medium (jacobsite and iwakiite) and large nodules (tephroite and bixbyite), (ii) the appearance of a Mn-rich internal core in the medium and large nodules, and (iii) the crystallinity of the core in the large nodules (3–5 mm). These observations led us to suggest that the primary Mn-Fe-containing minerals are the key factors (at least for Udepts) that affect not only the growth of the nodules but also the formation of their reactive matter and enrichment by trace elements.

Abbreviations: EDX, energy dispersive X-ray fluorescence spectroscopy; EF, enrichment factor; SEM, scanning electron microscopy.

Iron-Mn nodules occur in soils of different origins from many bioclimatic zones and act as specific filters for soil self-purification (Latrille et al., 2001; Cornu et al., 2005; Hickey et al., 2008; Gasparatos, 2013). The nodules consist of different combinations of Fe and Mn oxides (the major compounds in the nodules). The nodules are also characterized by a high exchange capacity and a well-defined sorption activity for trace elements (McKenzie, 1980; Liu et al., 2002; Dowding and Fey, 2007; Gasparatos et al., 2005; Cornu et al., 2009). Trace elements differ in their selectivity for sorption by the Fe-Mn compounds in the nodules. Trace element partitioning between the Fe and Mn oxides is characterized by specific peculiarities (Palumbo et al., 2001; Liu et al., 2002; Negra et al., 2005). Based on these peculiarities, trace elements can be divided into Mn and Fe groups (Manceau et al., 2002, 2003; Neaman et al., 2004; Cornu et al., 2009). The trace elements tend to concentrate in the mineral phase of nodules (i.e., the fine fraction minerals (ferrihydrite), mixed-layer minerals (lithiophorite), and layer minerals (birnessite)) (Liu et al., 2002; Manceau et al., 2002, 2003). Redox cycles and pH

this article has online supplemental material.

Soil Sci. Soc. Am. J. 78:767–778
doi:10.2136/sssaj2013.10.0444
Received 21 Oct. 2013.

*Corresponding author (timofeeva@biosoil.ru).

changes can affect the properties of the major Fe-Mn compounds in the nodules and of their associated trace elements (Cornu et al., 2009; Sipos et al., 2011).

Several studies have reported on alterations in the contents of trace elements in nodules of different sizes (Timofeeva, 2008; Gasparatos, 2013). However, most studies have been conducted using average nodule samples. Average test samples cannot provide comprehensive information about the specific sorption properties of the nodules. Nodules of different sizes are present in different soils and can be classified as very fine, fine, medium, and large. It is reasonable to suggest that nodules of various sizes should differ in their internal structures, mineralogy, and ratio of Fe to Mn. It has been reported that the content of Mn, Fe, crystalline Mn oxide, and Fe oxide increases in larger nodules (>2 mm) whereas the Fe/Mn ratio decreases (Zhang and Karathanasis, 1997; Aide, 2005). However, there are presently no comprehensive studies on this issue.

We examined uncontaminated Udepts from the west coast of the Pacific Ocean (the Primorye Region of Far East Russia). Most studies on nodules from the Pacific region (e.g., from China, Japan, Taiwan, and the Far East of Russia) have been performed on anthropogenically impacted soils. In most cases, these soils were tillable (Liu et al., 2002; Arachchi et al., 2004; Timofeeva, 2008; Jien et al., 2010). Udepts that form in uncontaminated fields are ideal materials for investigating the migratory cycles of trace elements in the pedosphere under natural conditions. In general, Udepts are freely drained soils characterized by either udic or perudic moisture regimes (Soil Survey Staff, 1999). Udepts from the west coast of the Pacific are subjected to the influence of the monsoon climate, with cyclic alternative wet and dry periods. These soils contain hard, brown, spherical nodules of different sizes (Timofeeva and Golov, 2007). Similar nodules have been found in Ultisols formed in the coastal regions of Taiwan, the Alfisols of Missouri and Kentucky, and in the hydromorphic soils of the Amazon (Zhang and Karathanasis, 1997; Aide, 2005; Jien et al., 2010; Coringa et al., 2012).

The objective of this study is to identify the specific interelemental relationships of the major and trace elements in nodules of different sizes and to characterize their morphologies, mineralogies, and chemical compositions. We show that the levels of trace element accumulation, morphological features, and chemical and mineralogical compositions of the nodules varied significantly with the nodule size.

MATERIALS AND METHODS

Site Description

Soils and nodules were sampled from an unpolluted area on the coast of the Russian Far East. The uncontaminated field was located in the Kedrovaya Pad Natural Reserve (43°7′ N lat; 131°37′ E long) territory. The Kedrovaya Pad is a typical territory of the southern Ussuri taiga. It contains a large massif of virgin coniferous–broadleaved forests. Upper Cretaceous effusive rocks dominate this area. Their derivatives serve as the soil-forming material. The climate of this territory is characterized as monsoon. In January, north, north-west, and west winds dominate whereas in July, the winds are from the south, south-east, and east. The winter climate is arid, fair, and frosty, with an average daily air temperature of −17°C and humidities of 30 to 40%. The summer monsoon climate is cloudy and rainy with an average daily air temperature of 22°C and a humidity of less than 80%. Most downfalls occur from August to September when the typhoons bring in significant rains. The average long-term frost-free duration is 232 d, and the average temperature is +5°C. The hydrology is characterized by desiccation in the spring and humidification in the summer and beginning of autumn. During the highest humidity seasons, the top and subsurface soil horizons have redox amplitude changes of 400 mV or more (Boyarkin and Kostenkov, 2012).

Table 1. Mineralogical compositions of different nodule sizes.

Nodules	Minerals
1–2 mm	quartz, sillimanite, ferrosilite, hematite
2–3 mm	quartz, ferrosilite, jacobsite, iwakiite
3–5 mm	tephroite, bixbyite, quartz, sillimanite

Soil Characterization

The experimental soil fields are classified as Udepts according to U.S. Soil Taxonomy (Soil Survey Staff, 1999). The location of the soil favors regular saturation from atmospheric precipitation and surface runoff. Gley features (olive and whitish mottles) are absent in the soil profile, which points to short-term soil waterlogging. The selected chemical and physical properties of the Udepts are presented in Supplementary Table 1. The soils are characterized by significant weathering processes, which increase the accumulation of the clay fraction in the middle and lower parts of the soil profiles (Semal', 2010). The organic C content in these Udepts varies from 7.2 g kg^{-1} to 100.5 g kg^{-1}. The acidity of these soils vary from acidic (pH 4.8) to slightly acidic (pH 5.9).

Soil and Nodule Sampling

Soils and nodules were collected in June 2010 from two soil profiles. The soil profiles were divided into the following depths: 0 to 6 cm (horizon A), 6 to 13 cm (AB), 13 to 42 cm (Btc1), 42 to 68 cm (Btc2), and 68 to 84 cm (horizon BtC). The soil pits were dug by hand, and the nodules were sampled from the main genetic horizons (A, AB, Btc1, Btc2, and BtC). Soil samples (2000–3000 g) from each horizon were weighed to determine the nodule abundance. To extract Fe-Mn nodules from the soil matrix, the soil was wet sifted through a nylon screen with a fine mesh size (0.05 mm). The sieved nodules were dried at 105°C for 12 h. The nodules were separated into different size classes using different sets of sieves: 1 to 2 mm, 2 to 3 mm, and 3 to 5 mm. Nodules of all sizes were hand separated from the sediment and weighed. The nodule and soil samples were ground using an agate mortar and pestle to obtain a powder and passed through a sieve (0.06 mm). Before the X-ray spectroscopy measurements, the powder was pressed into tablets (3.5 g) using a pressure of 8 to 15 Mg. The tablets were placed on circular sheets of Mylar X-ray polyethylene film. For the organic elemental analysis, the pow-

ders were wrapped in tin capsules (5 by 8 mm). Approximately 1000 nodules samples (1–2 mm ~ 400; 2–3 mm ~ 300; 3–5 mm ~ 300) were analyzed using different elemental analysis methods. The samples were impregnated with an epoxide resin to examine the elemental distribution within the nodules. After hardening, the nodules within the impregnated blocks were cut in half. Elemental distribution maps were created using 14 samples for the 1- to 2-mm nodules, nine samples for the 2- to 3-mm nodules, and six samples for the 3- to 5-mm nodules. For scanning electron microscopy, 30 samples of each size were prepared by vacuum coating the surface with Au for analysis.

Elemental Analysis

The total SiO_2, Al_2O_3, TiO_2, CaO, MgO, and K_2O contents were determined using energy dispersive X-ray fluorescence spectroscopy (EDX). Energy dispersive X-ray fluorescence spectroscopy analysis was performed with a Shimadzu EDX-800HS-P instrument (Shimadzu EUROPA GmbH) equipped with a rhodium X-ray tube (settings: vacuum, voltage 50 kV, current 100 μA, detection time 300 s, dead time 20%, and a collimator of 10 mm). The data were analyzed using PCEDX Shimadzu software. The elements were measured by K-line emission. Six certified reference standard samples (901-76, 902-76, 903-76, 2498-83, 2499-83, 2507-83) from the Institute of Applied Physics of Irkutsk State University were used to obtain calibration curves and to assess the analytical recovery and precision. One standard soil sample (2507-83) was included for every five unknown samples. The certified values for the standard soil were as follows: SiO_2 (71.49%), Al_2O_3 (9.81%), TiO_2 (0.74%), CaO (1.60%), MgO (0.95%), and K_2O (2.42%). Acceptable recoveries for the standards were ±13% of the certified values.

The total Fe, Mn, Co, Ni, Zn, Cu, and Pb contents of the soils and nodules were determined by atomic absorption spectrometry (Atomic Absorption Spectrophotometer AA-7000, Shimadzu). The samples were completely dissolved in HF and HNO_3 and analyzed as previously described (Sawhney and Stilwell, 1994).

Elemental distribution maps were obtained from electron probe microanalysis (Electron Probe Microanalyzer JXA-8100, Jeol). The analysis of the distribution of different elements within the nodules was performed at 30 kV using a working distance of 11 mm and a spot size of 2 μm.

Organic elemental analysis (total C and N) was performed using a Flash 2000 elemental analyzer (Thermo Scientific) with a CHNS configuration. Elemental data were analyzed using the Eager Xperience software. The samples were analyzed in a quartz reactor at 900°C with a column temperature of 65°C. The helium and oxygen flow rates into the reactor were 140 mL min^{-1} and 100 mL min^{-1}, respectively. The time cycle was 380 s, and the oxygen injection time was 15 s. The organic analytical standard for Cystine (OAS 134139) and the K Factor calibration method were used for quality control.

X-ray Diffraction Analysis

X-ray diffraction (XRD) was used to determine the mineral compositions of whole nodules of each size. The samples were analyzed using a Rigaku MiniFlexII X-ray diffractometer (Rigaku) from 2.5° to 60° 2Θ. The X-ray diffraction analysis was conducted using Cu-Kα radiation generated at 30 kV and 15 mA using a monochromator (with the SC attached) on the counter arm and a continuous scan speed of 1° 2Θ min^{-1} with a 0.02° 2Θ average count interval, a 1.25° divergence slit, a 0.3-mm receiving slit, and a 1.25° scatter slit. The International Centre for Diffraction Data 2010 database was used to determine the phases present in the nodules based on comparison of the diffraction patterns.

Scanning Electron Microscopy

The nodules were imaged using a field-emission scanning electron microscope (EVO 40, Carl Zeiss SMT). The scanning electron microscopy (SEM) images were recorded at magnifications of 2 to 719× using extra high tension at 5 to 20 kV, a low probe parameter for current and working distances of 15 to 30 mm. The SEM signal was SE1. Images were collected from selected areas of the nodule sections.

Statistical Methods

Each analysis was performed with three parallel probes to identify the adequate iteration number. The data were processed statistically (median value and regression analyses) using Microsoft Excel and SPSS software (SPSS Inc., version 16, 2007). Analysis of variance was used to determine significant differences and correlation matrices for the trace elements, Mn and Fe. The significance level (P) did not exceed 0.05. The enrichment factor (Kx) was calculated from the data for the bulk elemental contents as the ratio of element (x) concentration in the nodules to its concentration in the soil (without considering the nodules): $Kx = Cnod/Csoil$ (Gasparatos, 2013).

RESULTS

Nodules Morphology and Mineralogy

The Udepts contained abundant rounded and ellipsoid-shaped smooth nodules of different sizes. Most nodules exist as hard compact segregations, but the 1- to 2-mm nodules could be easily crushed by hand. All of the nodules had two zones, an outer zone and an internal zone, that could be easily identified by color. Each nodule fraction was characterized by a unique surface and internal structural features. The outer surfaces of the unbroken nodules were brown (7.5YR 4/4) to reddish-brown (2.5YR 4/4) and dark reddish-brown in color (2.5YR 2.5/4). The surfaces were shiny in appearance when the soil matrix was washed off. The internal parts of the nodules were heterogeneous with granular structures and nonconcentric layers (Fig. 1). The internal parts of the nodules were dark brown (7.5YR 3/3) with reddish-black (2.5YR 2.5/1) and black (7.5YR 2.5/1) areas of different shapes and sizes. The colors of the different zones of the nodules depended on the content of Fe and Mn, illustrating the dynamic precipitation process of the major com-

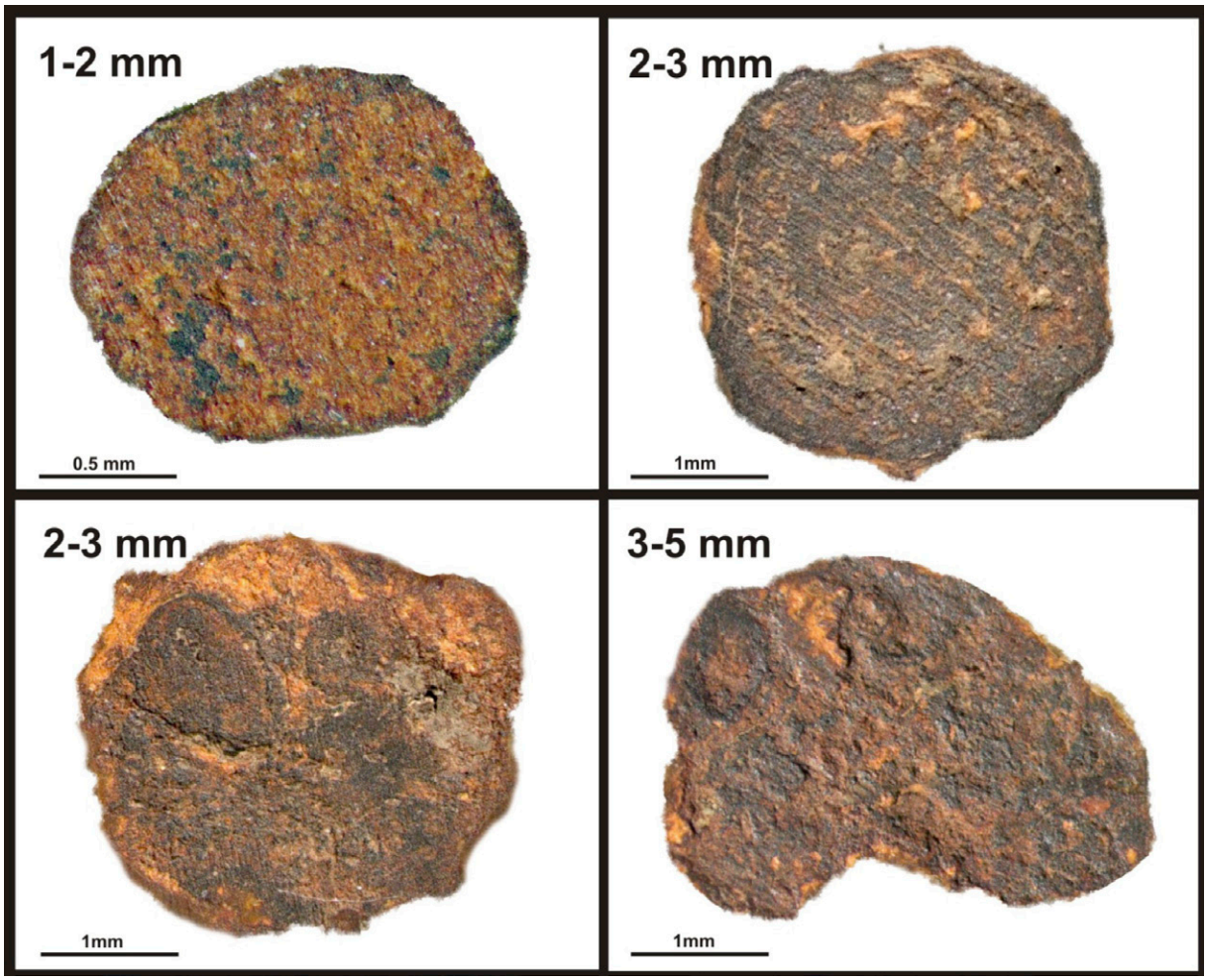

Fig. 1. Morphologies of opened nodules of different sizes.

pounds of the nodules, as previously described (Rhoton et al., 1993; Zhang and Karathanasis, 1997; Liu et al., 2002). As a rule, the black areas within the nodules contained higher amounts of Mn (Zhang and Karathanasis, 1997; Jien et al., 2010). Our results show that nodules of all sizes have C-rich black areas (Fig. 2). These areas were different sizes and were disconnected from each other. The C-rich black areas were found both in the center and in the outer zones of the nodules.

Nodules Measuring 1 to 2 mm

The surface of the nodules consisted of two layers (Fig. 3a). The first layer contained numerous planar, acute-angled plates. The second layer was porous and consisted of tightly packed plates that formed a homogenous rough mass. The internal zone was dark brown (7.5YR 3/3) with the incorporation of single granules that appeared as C-rich black (7.5YR 2.5/1) areas (Fig. 1 and 2). An investigation of the nodule mineral composition showed that the fine nodules (1–2 mm) served as cementation zones for Fe and Mn compounds. The mineral phases of the nodules were largely represented by primary minerals (Table 1; Supplementary Figure 1). Hematite was observed in smaller quantities at a proportion of 1 (hematite):6 (quartz, sillimanite and ferrosilite).

Nodules Measuring 2 to 3 mm

The surfaces of these nodules were more compact, containing layers and smooth, small, spherical formations (Fig. 3b). The friable internal zones of these nodules had intermixed dark brown (7.5YR 3/3), reddish-black (2.5YR 2.5/1), and black (7.5YR 2.5/1) coloring (Fig. 1). A visual inspection of the internal zones showed two different distributions for the dark-colored matter. The first type of distribution was characterized by an equal, circular distribution of isolated dark-colored matter and by the presence of reddish-yellow (7.5YR 6/8) areas (Fig. 1). The second type of distribution had large, rounded areas of dark-colored matter (usually three to four areas) (Fig. 1). The center and outer parts of these areas were reddish-black (2.5YR 2.5/1) separated by dark brown regions (7.5YR 3/3). The first type of distribution tended to occur for 2- to 2.5-mm nodules. The second type of distribution occurred more frequently for nodules larger than 2.5 mm.

The presence of a Mn-rich inner core was the main difference in the internal structure of the 2- to 3-mm nodules compared to the 1- to 2-mm small nodules (Fig. 2). Quartz, ferrosilite, and two Mn-Fe-containing minerals (jacobsite and iwakiite) were the primary minerals in the 2- to 3-mm nodules (Table 1; Supplementary

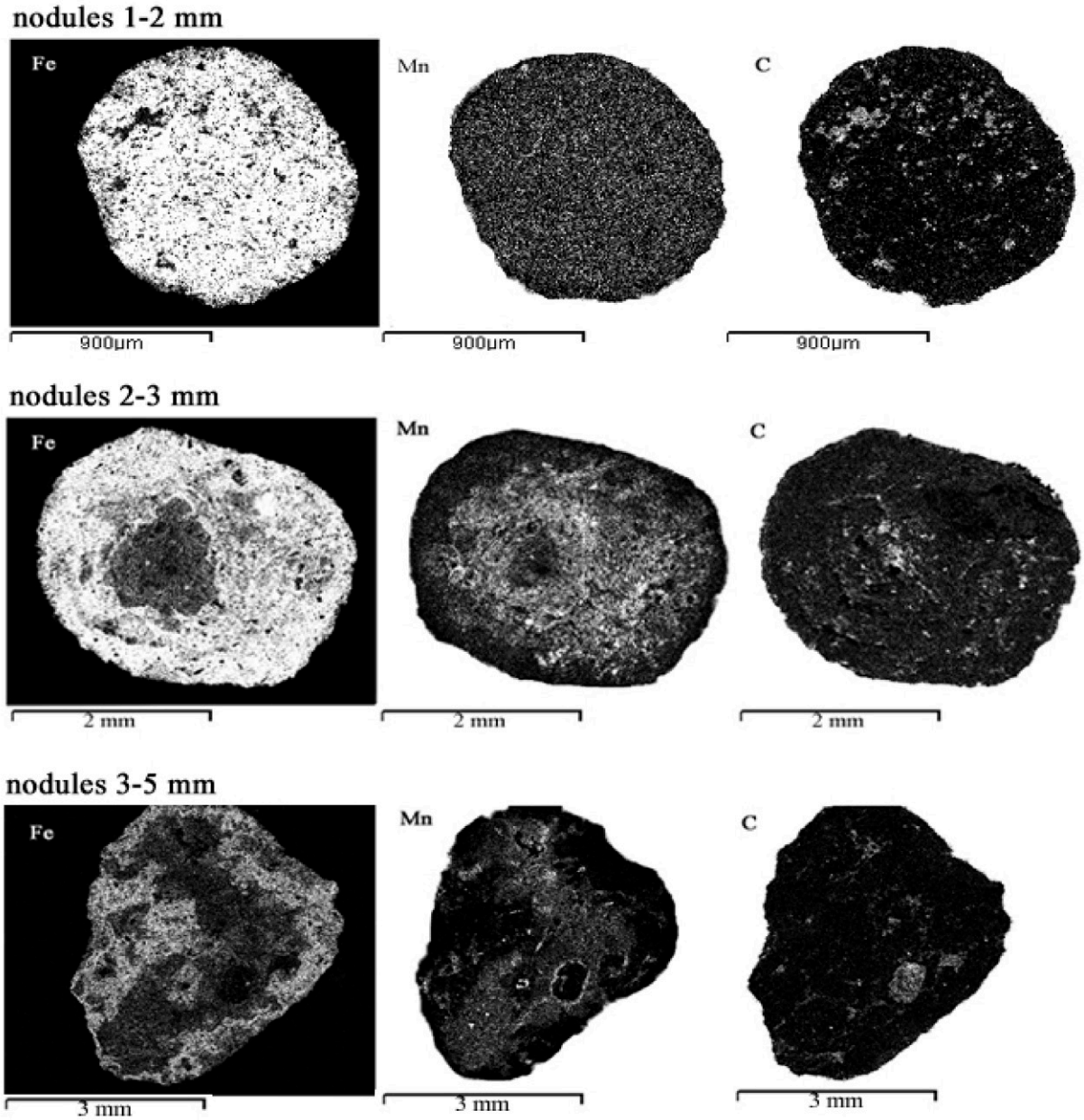

Fig. 2. Iron, Mn, and C distribution maps for different nodule size fractions.

Figure 1). Notably, the quartz and ferrosilite content in the 2- to 3-mm nodules was lower than in the smaller nodules.

Nodules Measuring 3 to 5 mm

The uneven surfaces of the large nodules resembled a moonscape (Fig. 3c). There were rare branching cracks on the surface. The surfaces of these nodules had thin-layered structures (Fig. 3c and 3d). The thickness of the outer zones of the nodules ranged from 20 to 420 μm, and a clearly defined boundary was observed between the outer and internal zones of the nodules (Fig. 3d). The internal zones of the nodules were intermixed with dark brown (7.5YR 3/3), reddish-black (2.5YR 2.5/1), and black (7.5YR 2.5/1) colors separating large rounded areas. In most cases, the rounded areas were similar to those observed in the 2- to 3-mm nodules. The internal zones of the nodules contained geometric structures that resembled parallel-oriented opaque crystals (Fig. 3d and 3e). The crystals had elongated cubical, triangulate, and flat columns. The crystal surfaces were rough around the crack. The lateral sides were covered by individual mineral films and flaky formations. The larger nodules (3–5 mm) were enriched with Mn-Fe-containing minerals, such as tephroite and bixbyite at a proportion of 1 (quartz and sillimanite):4 (tephroite and bixbyite) (Table 1; Supplementary Figure 1). The content of quartz and sillimanite was lowest for the 3- to 5-mm nodules.

Nodule Abundance

The quantitative distribution of nodules in the soil was characterized by a consecutive increase from the upper (horizons A, AB) to the middle parts (horizons Btc1, Btc2) of the soil profile. The peak abundance was observed in the middle part. The number of nodules sharply decreased in the lower part (horizon

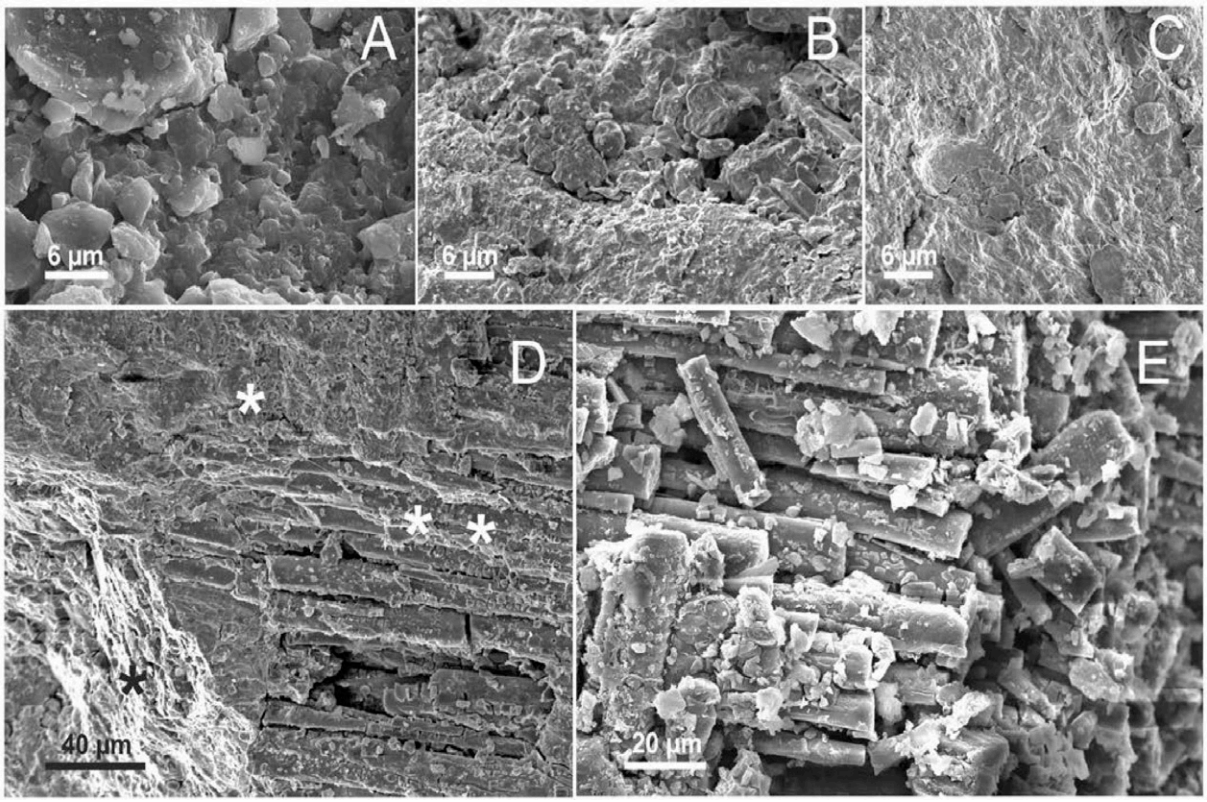

Fig. 3. Scanning electron microscopy images of the nodules: (a) 1- to 2-mm nodule surface, (b) 2- to 3-mm nodule surface, (c) 3- to 5-mm nodule surface, (d) micromorphology of the 3- to 5-mm nodules showing the structure of the nodule outer zone (*) and the structure of the nodule internal zone (**), and (e) close-ups of the internal zones of the 3- to 5-mm nodules showing the parallel-oriented crystals with mineral films on the lateral sides.

BtC), with the lowest amount occurring at a depth of 68 to 84 cm (Fig. 4). Nodules of 2 to 3 mm in size were the primary type found. We observed a clear dependence between nodule size and nodule depth in the soil. The upper horizon (A) contained mainly brown (7.5YR 4/4) and reddish-brown (2.5YR 4/4) 2- to 3-mm nodules, along with a smaller proportion of nodules smaller than 2 mm. The abundance of nodules in the deeper horizons (AB, Btc1, Btc2) increased due to an increase in the total amount of 1- to 2-mm and 2- to 3-mm nodules and the appearance of large dark reddish-brown (2.5YR 2.5/4) 3- to 5-mm nodules. The greatest amount of 3- to 5-mm nodules occurred in the Btc2 horizon. The content of nodules decreased in the deepest zone of the soil profile (BtC) where nodules of 1 to 2 and 2 to 3 mm were the most common.

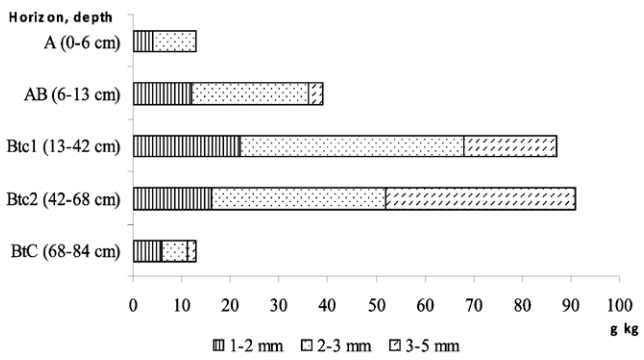

Fig. 4. Abundance of different nodules size fractions in the Udepts.

Elemental Analysis
Macroelements

The nodule chemistry is presented in Table 2, Table 3, and Fig. 5. The main elements found in the nodules were Si, Al, Fe, K, Mg, C, and Mn. The content of all other elements was less than 0.5%. The analysis of the elemental oxides revealed low concentrations of SiO_2 and MgO in the nodules. In contrast to our nodules, soil nodules from other sites had considerably higher concentrations of SiO_2 (43–57%) and MgO (1.3–11.9%) (Tan et al., 2006; Gasparatos, 2013). In general, the levels of these elemental oxides in our nodule samples were lower than those in the surrounding soils. This result suggests that SiO_2, Al_2O_3, TiO_2, CaO, MgO, and K_2O were components of the trapped soil materials, according to the rule described by Zhang and Karathanasis (1997) and Liu et al. (2002). Nodules of 3 to 5 mm were the exception to this rule, as they contained higher concentrations of TiO_2 than those found in other soils.

The concentration of elemental oxides was dependent on the nodule size. The abundance of macroelement oxides was slightly different between the 1- to 2-mm nodules and the 2- to 3-mm nodules. The 3- to 5-mm nodules contained higher concentrations of SiO_2, Al_2O_3, TiO_2, CaO, MgO, and K_2O than the smaller nodules did. The increase in nodule size from 1 to 2 mm to 2 to 3 mm was most likely associated with the accumulation of major nodule compounds.

Iron appears to play the main role in this process. It is evident from Fig. 5 that the concentrations of Mn and Fe in the nodules are related to the nodule size. The concentration of Fe was the highest in the 2- to 3-mm nodules. The lowest Fe level was observed in the large (3–5 mm) nodules. In contrast, the concentration of Mn in the nodules increased with the nodule size. The relationships between Mn and Fe in the fine, medium, and large nodules were also different. In the 1- to 2-mm and 2- to 3-mm nodules, Fe-containing compounds were more common than Mn-containing compounds. In nodules of these sizes, the total concentration of Fe was higher than the total concentration of Mn. The formation of 3- to 5-mm nodules correlated to an increase in the amount of Mn-containing compounds. The 3- to 5-mm nodules contained more Mn than Fe. The trends observed for the Mn and Fe concentrations were closely associated with the values describing the enrichment factors for elements in nodules of different sizes. Generally, nodules of all sizes concentrate Mn (enrichment factor 4.7–71) and Fe (enrichment factor 1.5–13.4). The enrichment factor for Mn (33–71) was the highest in the 3- to 5-mm nodules. The enrichment factor for Fe (7.2–13.4) was the highest in the 2- to 3-mm nodules.

Table 2. Oxide content of different nodule sizes and the surrounding soil based on energy dispersive X-ray spectroscopy analysis and C and N elemental analysis.

Element	Soil	Nodules		
		1–2 mm	2–3 mm	3–5 mm
		%		
SiO_2	71.09 ± 4.36†	36.61 ± 2.79	37.79 ± 2.39	42.73 ± 3.19
Al_2O_3	15.26 ± 2.11	7.28 ± 1.02	7.1 ± 0.94	9.73 ± 1.42
TiO_2	0.72 ± 0.15	0.49 ± 0.13	0.57 ± 0.14	0.99 ± 0.14
CaO	1.50 ± 0.34	0.41 ± 0.09	0.40 ± 0.12	1.07 ± 0.22
MgO	1.36 ± 0.21	0.71 ± 0.15	0.73 ± 0.14	0.96 ± 0.21
K_2O	2.44 ± 0.39	1.48 ± 0.34	1.59 ± 0.47	2.07 ± 0.46
C	3.17 ± 0.53	0.83 ± 0.11	1.29 ± 0.14	1.68 ± 0.23
N	1.26 ± 0.27	0.16 ± 0.07	0.24 ± 0.09	0.30 ± 0.11

† Mean values ± standard deviations.

Trace Elements

The average abundance of trace elements in the studied Udepts was as follows: Ni > Cu > Zn > Co > Pb (Table 3). Investigations of the depth profiles demonstrated that the concentrations of Ni, Cu, Zn, and Co were the highest at surface horizon A. According to Nowack et al. (2001), greater concentrations of metals in the upper horizon relate to the cycling of metals in the soil–plant environment. The concentration of Pb increased with depth, and the highest amount was found in the middle part of the soil profile (horizons Btc1, Btc2).

The 1- to 2-mm nodules had stable, low concentrations of trace elements, accompanied by low enrichment factor (EF) values. The EF for the trace elements in the fine nodules varied from 0.1 to 0.7. Such values indicate a very slow accumulation of trace elements in these nodules. Further increases in the trace element concentrations in the nodules were correlated to significant increases in accumulation capacity.

The 2- to 3-mm and 3- to 5-mm nodules contained high concentrations of Co (EF 3.2–8.7), Ni (EF 1.7–3.5), Cu (EF 1.7–2.8), and Pb (EF 1.4–2.6). The accumulation of Zn (EF 1.4–2.2) was only observed in the large nodules. The concentrations and EFs for trace elements peaked in the 3- to 5-mm nodules. The levels of trace elements in the nodules varied with depth.

Table 3. Trace element compositions of different nodule sizes and the surrounding soil based on atomic absorption spectrometry analysis.

Element	Object		A (0–6 cm)	AB (6–13 cm)	Btc1 (13–42 cm)	Btc2 (42–68 cm)	BtC (68–84 cm)
			mg kg^{-1}				
Co	soil		16.73 ± 0.92†	13.42 ± 0.61	14.80 ± 1.12	15.12 ± 0.70	6.17 ± 0.42
	nodules	1–2 mm	7.61 ± 0.64	8.15 ± 0.54	7.96 ± 0.51	7.29 ± 0.88	4.30 ± 0.48
		2–3 mm	54.28 ± 3.90	72.82 ± 5.01	99.02 ± 5.43	87.17 ± 3.83	15.55 ± 1.91
		3–5 mm	84.05 ± 4.21	92.86 ± 3.32	128.59 ± 6.08	136.90 ± 5.51	21.90 ± 2.21
Ni	soil		27.56 ± 1.20	26.17 ± 1.94	22.83 ± 1.36	22.36 ± 1.54	11.06 ± 1.29
	nodules	1–2 mm	2.91 ± 0.36	3.06 ± 0.68	5.28 ± 0.62	4.82 ± 0.58	0.79 ± 0.16
		2–3 mm	51.11 ± 3.07	44.74 ± 1.72	53.19 ± 1.92	49.71 ± 2.37	14.61 ± 0.75
		3–5 mm	57.19 ± 3.70	62.63 ± 3.35	75.80 ± 7.06	77.72 ± 6.38	19.61 ± 2.30
Cu	soil		24.64 ± 2.12	17.74 ± 1.62	22.37 ± 2.11	23.17 ± 2.06	8.56 ± 0.90
	nodules	1–2 mm	4.68 ± 0.55	2.69 ± 0.31	1.96 ± 0.32	2.19 ± 0.48	3.64 ± 0.70
		2–3 mm	41.46 ± 2.65	47.26 ± 2.84	51.62 ± 3.10	29.90 ± 2.42	14.38 ± 1.16
		3–5 mm	51.28 ± 4.12	48.25 ± 2.60	52.16 ± 3.42	54.76 ± 4.42	23.62 ± 1.98
Zn	soil		21.18 ± 2.46	19.87 ± 1.06	20.19 ± 2.24	17.09 ± 1.30	17.68 ± 2.61
	nodules	1–2 mm	2.50 ± 0.37	0.93 ± 0.21	4.63 ± 0.27	5.14 ± 0.72	1.88 ± 0.36
		2–3 mm	2.92 ± 0.21	5.50 ± 0.44	9.34 ± 1.29	5.32 ± 0.76	12.49 ± 1.61
		3–5 mm	29.08 ± 1.70	33.72 ± 1.10	27.61 ± 0.98	24.39 ± 1.72	39.66 ± 3.80
Pb	soil		12.69 ± 0.51	9.96 ± 0.87	15.33 ± 1.76	14.86 ± 1.14	11.17 ± 2.45
	nodules	1–2 mm	1.43 ± 0.20	1.64 ± 0.33	2.49 ± 0.55	1.82 ± 0.40	1.18 ± 0.39
		2–3 mm	13.77 ± 1.24	16.32 ± 2.21	25.16 ± 1.94	20.66 ± 2.41	13.80 ± 1.61
		3–5 mm	29.42 ± 3.61	25.61 ± 2.08	30.07 ± 2.49	35.51 ± 1.91	19.24 ± 0.85

† Mean values ± standard deviations.

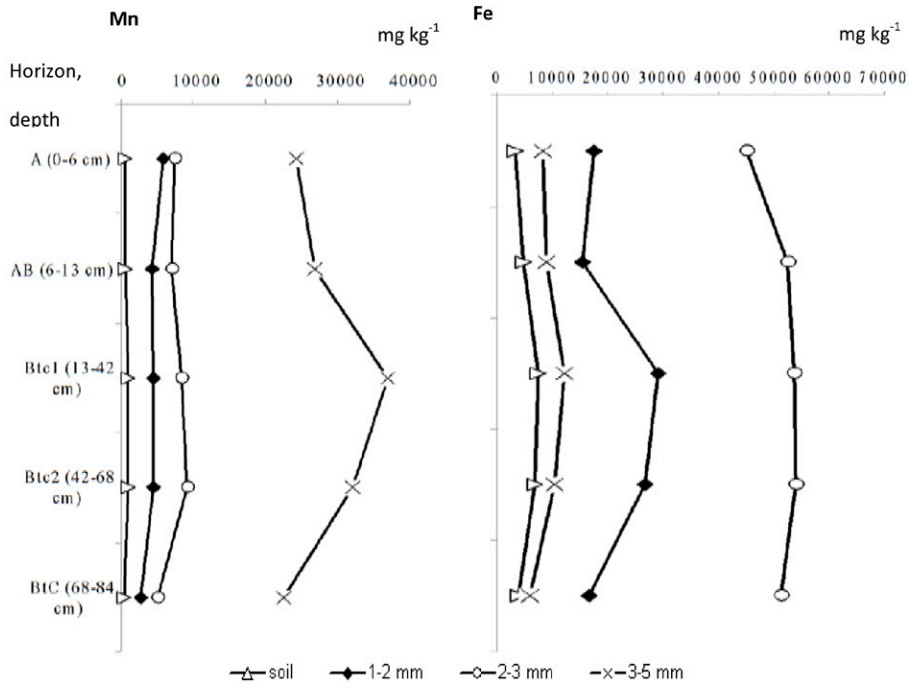

Fig. 5. Different nodule size fractions and surrounding soil concentrations of Mn and Fe.

The accumulation of Co and Ni increased for nodules located in the middle part of the profile (horizons Btc1, Btc2). Lead and Cu mainly concentrated in nodules located in the subsurface (horizon AB). Zn concentrations were higher in nodules in the underlying horizon (BtC).

An analysis of the relationship between the concentrations of the major compounds in the nodules and the concentrations of the trace elements revealed a complex relationship for nodules of different sizes (Fig. 6). For the 1- to 2-mm nodules, the Pb and Zn contents strongly correlated to the amount of Fe ($r_{Fe\text{-}Zn}$ 0.95; $r_{Fe\text{-}Pb}$ 0.85). The concentrations of Co were significantly correlated to Mn ($r_{Mn\text{-}Co}$ 0.76), and Mn had a positive correlation with Cu ($r_{Mn\text{-}Cu}$ 0.5).

The relationship of the elements changed with increasing nodule size. The association of Mn with trace elements increased in the 2- to 3-mm nodules compared to the 1- to 2-mm nodules. The concentration of Mn was significantly correlated to the concentrations of Co, Ni, and Pb ($r_{Mn\text{-}Co}$ 0.9; $r_{Mn\text{-}Ni}$ 0.86; $r_{Mn\text{-}Pb}$ 0.73). The interelemental relationship of Mn with Cu was similar to that observed for fine nodules.

In the large nodules, the accumulation of trace elements was controlled by Fe-containing compounds. The associations of trace elements in the nodules indicated that the concentrations of Co and Ni ($r_{Fe\text{-}Co}$ 0.94; $r_{Fe\text{-}Ni}$ 0.93) strongly correlated with the amount of Fe. Likewise, Fe correlated with Cu, Zn, and Pb ($r_{Fe\text{-}Cu}$ 0.82; $r_{Fe\text{-}Zn}$ 0.8; $r_{Fe\text{-}Pb}$ 0.78). For the large nodules, the significant correlation between Mn and elements associated with Mn-containing compounds was valid ($r_{Mn\text{-}Co}$ 0.84; $r_{Mn\text{-}Ni}$ 0.80) and similar to that observed in the small nodules.

Significant correlations were found among the concentrations of the trace elements for all the nodule sizes (Supplementary Table 2). The concentrations of Ni, Cu, and Zn in the nodules were found to significantly correlate with the Co content. The Pb and Zn concentrations in the nodules were the most dependent on the Cu levels. Additionally, significant correlations were observed between the Pb and Zn concentrations.

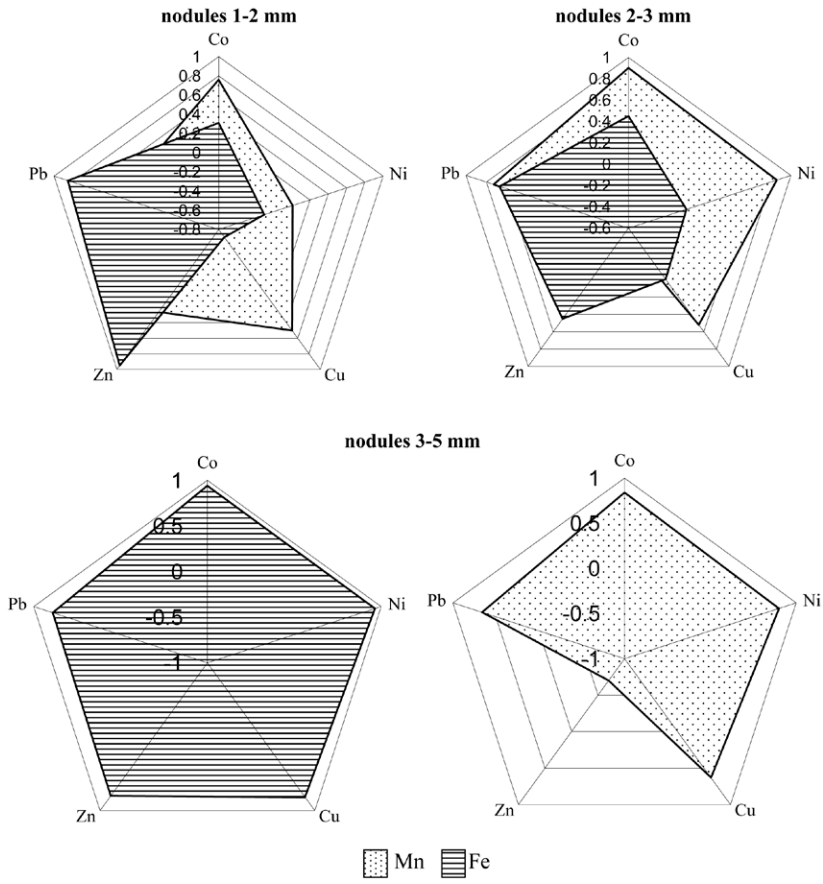

Fig. 6. Correlation coefficients between the concentrations of Fe, Mn, and trace elements for different nodule size fractions.

Carbon–Nitrogen

The total content of C and N in the nodules was less than that observed in the surrounding soil (Table 2). The content of these elements increased with increasing nodule size. Morphological observations and maps of the C distribution

showed that these elements concentrated at specific areas within the nodules (Fig. 1 and 2).

DISCUSSION

The nodule size distributions depended on the sampling locations in the soil profile (Fig. 4). The analysis of the nodule distribution revealed that the optimum conditions for nodule formation are in the middle part of the soil profile (horizons Btc1, Btc2). It should be noted that even under these optimal conditions, the size of the nodules did not exceeded 5 mm. The nodules analyzed in other studies varied from 0.2 to more than 20 mm (Zhang and Karathanasis, 1997; Liu et al., 2002; Jien et al., 2010; Gasparatos, 2013). Jien et al. (2010) reported that higher organic matter in the surrounding soil leads to the formation of smaller nodules. They concluded that the organic matter slows the crystallization of Fe oxide, which is required for the formation of large nodules. In this respect, our results are in agreement with those from Jien et al. However, we found that large nodules (3–5 mm) were not formed in the poorest organic matter horizons of the Udepts. Additional factors most likely affected the formation of the large nodules, such as the presence of C in the C-rich zones inside the nodules.

Iron–Manganese Compounds in Nodule Formation

Our data indicate that nodules of all sizes are composed of a complex Mn-Fe-oxide matrix, as well as soil mineral grains and C-rich areas (Fig. 2). A previous study showed that mineral grains of the soil matrix are composed of quartz, sillimanite, and ferrosilite, which are inert in the nodules and weakly transformed (Manceau et al., 2003; Timofeeva, 2008; Schulz et al., 2010). An important observation from the present work is that the specific capacity of trace element accumulation, morphological characteristics, and composition of the Mn-Fe-containing minerals of the nodules vary strictly with nodule size (Fig. 1–3 and 6; Table 3). The composition of the Mn-Fe-containing minerals changes depending on the nodule size in order of hematite (1–2 mm), jacobsite and iwakiite (2–3 mm), and tephroite and bixbyite (3–5 mm) (Table 1; Supplementary Figure 1). Tephroite (olivine group), jacobsite, and iwakiite (spinel group) are from different groups of metamorphic and metasomatic rocks. As previously shown, these minerals were inherited from the adjacent soil matrix (Abs-Wurmbach and Peters, 1999).

Hematite and bixbyite are products of the formation of minerals from primary solid solutions (Singh and Gilkes, 1996; Bevan and Martin, 2008). As reported in the literature, bixbyite has not been previously identified in nodules. Hematite has been found in nodules from different territories (Singh and Gilkes, 1996; Gaiffe and Kubler, 1992; Gasparatos et al., 2004; Vodyanitskii, 2010).

It was previously reported that the basic minerals composing the Mn-oxides in the nodules consist of birnessite, lithiophorite, and vernadite and that nodules of different sizes are mineralogically similar to each other (Liu et al., 2002; Tokashiki et al., 2003; Manceau et al., 2003; Neaman et al., 2004; Jien et al., 2010; Coringa et al., 2012). Our results show that none of these crystalline Mn-oxides were found in nodules from the Udepts. At the same time, most of the large (3–5 mm) nodules exhibited a crystalline morphology in their internal zones. We found numerous parallel-oriented crystals in our samples (Fig. 3d and 3e). The distribution of elements showed that the crystals were composed of complexes of Mn and Fe (Fig. 2). In these complexes, the content of one element increases as a function of the content of the other element and vice versa (Fig. 7a). We concluded that these crystal structures have not been previously found in nodules. Presently, the mineral associated with these types of crystal structures is not identified. In contrast to the crystal structures of the internal zones, the outer zones of the large nodules had layered structures (Fig. 3d). The outer zone consisted mainly of Fe compounds that were depleted of Mn (Fig. 2). The Fe and Mn in the outer zones precipitated together (Fig. 7a).

Taken together, our results suggest that the formation of unknown minerals in the internal zones of the 3- to 5-mm

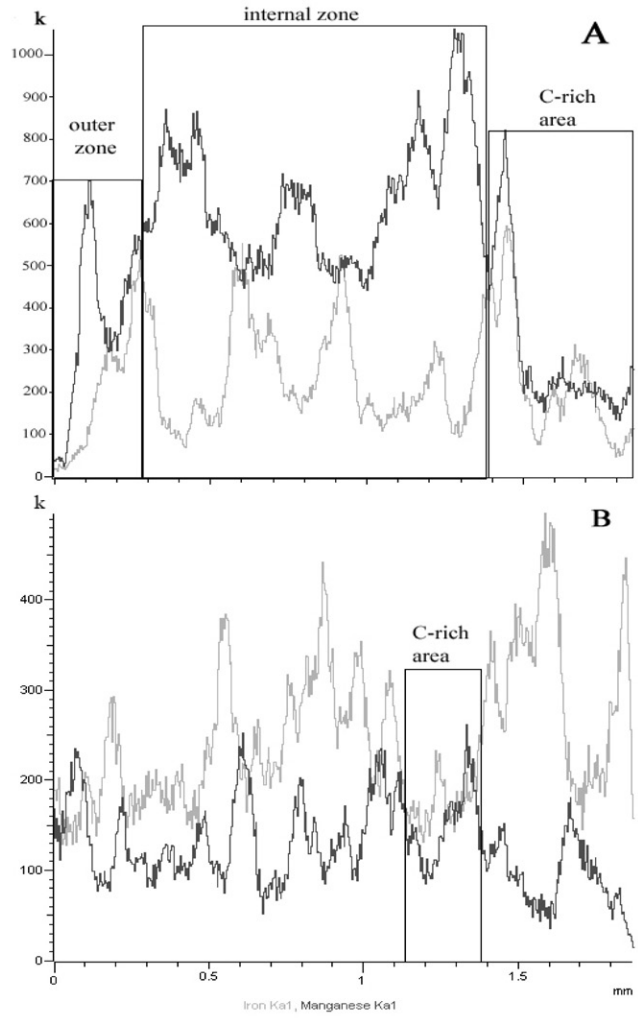

Fig. 7. Relationships between the concentrations of Fe and Mn within the 3- to 5-mm nodules (a) and the 2- to 3-mm nodules (b) showing the variability of precipitation elements in the different nodule zones. The light line represents the concentrations of Fe, and the dark line represents concentrations of Mn.

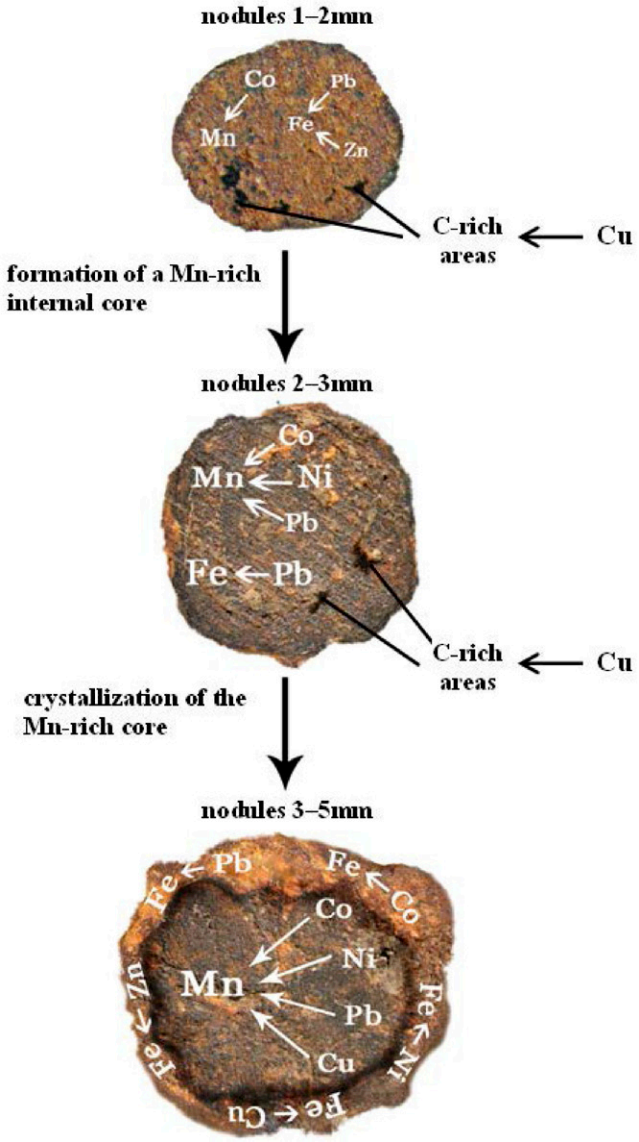

Fig. 8. Schematic diagram showing the variability of the association between trace elements and Fe and Mn during nodule formation and growth.

nodules might be the result of a combination of competing processes. One of these processes is the formation of compact forms of major compounds in the nodules due to Fe and Mn oxide and/or oxyhydroxide dehydration, which precipitates the surrounding soil into the outer zones of the nodules. The second process is the degradation of minerals (mainly tephroite) within the nodules. Evidence for primary mineral degradation within the nodules was found in nodules from the Santa Cruz terraces (Schulz et al., 2010). Schulz et al. (2010) also reported that the precipitated Fe-oxide within the nodules favored mineral dissolution. We also found evidence for mineral dissolution in the individual grains of the primary minerals in the nodules from each size fraction.

In contrast to the large nodules, the distribution of the major compounds in the fine nodules (1–2 mm) and the medium nodules (2–3 mm) showed that the concentration of one element was controlled by the content of another element during the formation of the common Fe-Mn phases (Fig. 7b). Some studies consider the homogeneous distribution of elements (without Fe-rich and Mn-rich zones) as one of the main features that distinguishes nodules from concretions. However, we observed an absence of specific element-rich zones for the 1- to 2-mm nodules (Fig. 2).

Different theories for nodule formation have been previously proposed. Most of these theories suggest that the initial stage of nodule formation involves the precipitation of Mn and Fe onto primary minerals. As a rule, the primary minerals in nodules are considered to be a base for the precipitation of oxidized Mn and Fe. In the nodules from the Udepts, we observed primary Mn-Fe-containing minerals in the medium nodules (2–3 mm) and in the large nodules (3–5 mm). The composition of these minerals varied with nodule size. Based on this observation, we propose that the primary Mn-Fe-containing minerals are an additional source for the main compounds of nodules. Most likely, they affect the formation of the reactive matter of the nodules and the enrichment by trace elements.

Trace Elements

Our investigations revealed different ratios for the major compounds to trace elements in the nodules depending on size. The variability of the association between trace elements and Fe and Mn during nodule formation and growth is depicted schematically in Fig. 8. In the 1- to 2-mm nodules, a positive correlation for Co, Pb, and Zn with Fe and Mn was observed. This peculiarity indicates the affinity of trace elements for amorphous or weakly crystallized compounds of Fe and Mn. In the fine nodules, Zn and Pb were associated with Fe, which is a single chemical phase-carrier for these elements. Cobalt was associated with the Mn phases in the fine nodules. The strong affinity between Co and Mn is frequently observed in nodules originating in different types of soils. A similar characteristic for the association between these elements was previously shown by Burgund Rendzine (France) in the Mississippi Cambisol (United States) and by Alfisol in Wuhan (China) soils (Liu et al., 2002; Manceau et al., 2002, 2003). In contrast to the common order for the association of Mn and Fe with trace elements, Ni was not correlated with the Mn phases in the fine nodules. The Cu content was negatively correlated with Fe. The Cu content was not correlated with Mn. The elemental distribution maps showed that Cu was mainly contained in the C-rich areas of the nodules (Supplementary Figure 2).

The relationships between these elements in the 2- to 3-mm nodules were different from those observed in the fine nodules. The 2- to 3-mm nodules had the highest Fe content of all the nodule fractions. However, the influence of this element on trace element accumulation was weaker than the influence of Mn. Iron was most likely contained in less reactive forms during formation of the combined complexes of Fe and Mn within the nodules. The concentrations of Co and Ni in the 2- to 3-mm nodules were controlled by their strong affinities for Mn. Lead was associated with Mn and Fe compounds. In nodules of this size, Mn and Fe

compounds played a secondary role in the accumulation of Zn and Cu. According to Manceau et al. (2003) and Vodyanitskiy (2005), Zn in nodules is concentrated in phyllosilicates, which were identified in our nodules. The Cu was concentrated in the C-rich areas (Supplementary Figure 2).

The accumulation capacity of the large nodules (3–5 mm) was largely dependent on the Fe compounds. The data for the distributions and associations of the elements indicate a possible reason for the decreasing amounts of reactive Mn forms with the formation of Mn-rich specific minerals in the internal zone of the nodules. Iron was mainly concentrated in the outer zone of the nodules and was the potential source for accumulation of trace elements. Based on the chemical composition and morphology of the large nodules, we propose a hypothesis for trace element accumulation. Iron is the primary accumulator for trace elements in the outer zones of the nodules. The transformation of the trace elements between the outer and internal zones occurs by forming solutions within thin films. These films saturate crystals forming inside the nodules and create a base for growing minerals. In the internal zone of the 3- to 5-mm nodules, Ni, Co, Cu, and Pb are predominantly associated with Mn compounds. In the 3- to 5-mm nodules, Zn is associated only with Fe compounds and is most likely contained in poorly crystallized Zn-containing iron phases.

ACKNOWLEDGMENTS

The analyses described in this work were performed using equipment from the Instrumental Centre for Biotechnology and Gene Engineering at the Institute of Biology and Soil Science and the Primorye Analytical Center for Local Element and Isotope Analysis at the Far Eastern Geological Institute. The authors thank their colleagues, especially Dr. Natalia Naryshkina and Dr. Tatyana Gorpenchenko for their valuable assistance with the microscopic investigations. This work was supported by grants 12-III-B-06-086 and 12-II-YO-06-012 from the Far Eastern Branch of the Russian Academy of Sciences.

REFERENCES

Abs-Wurmbach, I., and T. Peters. 1999. The Mn-Al-Si-O system: An experimental study of phase relations applied to parageneses in manganese-rich ores and rocks. Eur. J. Mineral. 11:45–68.

Aide, M. 2005. Elemental composition of soil nodules from two Alfisols on an alluvial terrace in Missouri. Soil Sci. 170:1022–1033. doi:10.1097/01.ss.0000187351.16740.55

Arachchi, L.P.V., Y. Tokashiki, and S. Baba. 2004. Mineralogical characteristics and micromorphological observations of brittle/soft Fe/Mn concretions from Okinawan soils. Clays Clay Miner. 52:462–472. doi:10.1346/CCMN.2004.0520407

Bevan, D.J.M., and R.L. Martin. 2008. The role of the coordination defect: A new structural description of four fluorite-related sesquioxide minerals, bixbyite (Mn2O3), braunite (Mn7SiO12), braunite II (CaMn14SiO24), parwelite (Mn10Sb2As2Si2O24), and their structural relationships. J. Solid State Chem. 181:2250–2259. doi:10.1016/j.jssc.2008.04.046

Boyarkin, R.D., and N.M. Kostenkov. 2012. Natural reserve Kedrovaya Pad. In: G.V. Dobrovol'skii, editor, Soil of nature reserves and national parks of Russian Federation. Infosphere Foundation–NIA-Priroda Press, Moscow. p. 399–401.

Coringa, O., E. de Arruda, C.E. Guimaraes, O. Perez, X. Luis, and T.P. Vidal. 2012. Attributes of the hydromorphic soils in the Pantanal of North Matogrosso. Acta Amazon. 42:19–28. doi:10.1590/S0044-59672012000100003

Cornu, S., J.A. Cattle, A. Samouëlian, C. Laveuf, L.R.G. Guilherme, and P. Alberic. 2009. Impact of redox cyclers on manganese, iron, cobalt, and lead in nodules. Soil Sci. Soc. Am. J. 73:1231–1241. doi:10.2136/sssaj2008.0024

Cornu, S., V. Deschatrettes, S. Salvador-Blanes, B. Clozul, M. Hardy, S. Branchut, and L. Le Forestier. 2005. Trace element accumulation in Mn-Fe-oxide nodules of a planasolic horizon. Geoderma 125:11–24. doi:10.1016/j.geoderma.2004.06.009

Dowding, C.E., and M.V. Fey. 2007. Morphological, chemical and mineralogical properties of some manganese-rich oxisols derived from dolomite in Mpumalanga province, South Africa. Geoderma 141:23–33. doi:10.1016/j.geoderma.2007.04.024

Gaiffe, M., and B. Kubler. 1992. Relationships between mineral composition and relative ages of iron nodules in Jurassian soil sequences. Geoderma 52:343–350. doi:10.1016/0016-7061(92)90045-9

Gasparatos, D. 2013. Sequestration of heavy metals from soil with Fe-Mn concretions and nodules. Environ. Chem. Lett. 11:1–9. doi:10.1007/s10311-012-0386-y

Gasparatos, D., C. Haidouti, and D. Tarenidis. 2004. Characterization of iron oxides in Fe-rich concretions from an imperfectly drained Greek soil: A study by selective-dissolution techniques and X-ray diffraction. Arch. Agron. Soil Sci. 50:485–493. doi:10.1080/0365034042000216149

Gasparatos, D., D. Tarenidis, C. Haidouti, and G. Oikonomou. 2005. Microscopic structure of soil Fe-Mn nodules: Environmental implication. Environ. Chem. Lett. 2:175–178. doi:10.1007/s10311-004-0092-5

Hickey, P.J., P.A. McDaniel, and D.G. Strawn. 2008. Characterization of iron- and manganese-cemented redoximorphic aggregates in wetland soils contaminated with mine wastes. J. Environ. Qual. 37:2375–2385. doi:10.2134/jeq2007.0488

Jien, Sh.-H., Z.-Ye. Hseu, and Z.-S. Chen. 2010. Hydropedological implications of ferromanganiferous nodules in rice-growing plinthitic Ultisols under different moisture regimes. Soil Sci. Soc. Am. J. 74:880–891. doi:10.2136/sssaj2009.0020

Latrille, C., F. Elass, F. van Oort, and L. Denaix. 2001. Physical speciation of trace metals in Fe–Mn concretions from a rendzic lithosol developed on Sinemurian limestones (France). Geoderma 100:127–146. doi:10.1016/S0016-7061(00)00083-5

Liu, F., C. Colombo, P. Adamo, J.Z. He, and A. Violante. 2002. Trace elements in manganese-iron nodules from a Chinese Alfisol. Soil Sci. Soc. Am. J. 66:661–670. doi:10.2136/sssaj2002.0661

Manceau, A., N. Tamura, R. Celestre, A. Macdowell, N. Geoffery, G. Sposito, and H.A. Padmore. 2003. Molecular-scale speciation of Zn and Ni in soil ferromanganese nodules from loess soils of the Mississippi Basin. Environ. Sci. Technol. 37:75–80. doi:10.1021/es025748r

Manceau, A., N. Tamura, M.A. Marcus, A.A. MacDowell, R.S. Celestre, R.E. Sublett, G. Sposito, and H.A. Padmore. 2002. Deciphering Ni sequestration in soil ferromanganese nodules by combining x-ray fluorescence, absorption, and diffraction at micrometer scale resolution. Am. Mineral. 87:1494–1499.

McKenzie, R.M. 1980. The adsorption of lead and other heavy metals on oxides of manganese and iron. Aust. J. Soil Res. 18:61–73. doi:10.1071/SR9800061

Neaman, A., B. Waller, F. Mouele, F. Trolard, and G. Bourrie. 2004. Improved methods for selective dissolution of manganese oxides from soils and rocks. Eur. J. Soil Sci. 55:47–54. doi:10.1046/j.1351-0754.2003.0545.x

Negra, C., D.S. Ross, and A. Lanzirotti. 2005. Soil manganese oxides and trace metals: Competitive sorption and microfocused synchrotron X-ray fluorescence mapping. Soil Sci. Soc. Am. J. 69:353–361. doi:10.2136/sssaj2005.0353

Nowack, B., J.M. Obrecht, M. Schluep, R. Schulin, W. Hansmann, and V. Koppel. 2001. Elevated lead and zinc contents in remote Alpine soils of the Swiss National Park. J. Environ. Qual. 30:919–926. doi:10.2134/jeq2001.303919x

Palumbo, B., A. Bellanca, R. Neri, and M.J. Roe. 2001. Trace metal partitioning in Fe–Mn nodules from Sicilian soils, Italy. Chem. Geol. 173:257–269. doi:10.1016/S0009-2541(00)00284-9

Rhoton, F.E., J.M. Bigham, and D.G. Schultze. 1993. Properties of ironmanganese nodules from a sequence of eroded fragipan soils. Soil Sci. Soc. Am. J. 57:1386–1392. doi:10.2136/sssaj1993.03615995005700050037x

Sawhney, B.L., and D.E. Stilwell. 1994. Dissolution and elemental analysis of minerals, soils and environmental samples. In: J.E. Amonette and L.W. Zelazny, editors, Quantitative methods in soil mineralogy. SSSA, Madison, WI. p. 49–82.

Schulz, M.S., D. Vivit, Ch. Schulz, J. Fitzpatrick, and A. White. 2010. Biologic

origin of iron nodules in a marine terrace chronosequence, Santa Cruz, California. Soil Sci. Soc. Am. J. 74:550–564. doi:10.2136/sssaj2009.0144

Semal', V.A. 2010. Properties of soils in southern Sikhote-Alin using the example of the Ussuri reserve. Euras. Soil Sci. 43:278–286. doi:10.1134/S1064229310030051

Singh, B., and R.J. Gilkes. 1996. Nature and properties of iron rich glaebules and mottles from southwest Australian soils. Geoderma 71:95–120. doi:10.1016/0016-7061(95)00092-5

Sipos, P., T. Nemeth, Z. May, and Z. Szalai. 2011. Accumulation of trace elements in Fe-rich nodules in neutral-slightly alkaline floodplain soil. Carpathian J. Earth Environ. Sci. 6:13–22.

Soil Survey Staff. 1999. Soil Taxonomy: A basic system of soil classification for making and interpreting soil surveys. U.S. Gov. Print. Office, Washington, DC.

Tan, W.F., F. Liu, Y.H. Li, H.Q. Hu, and Q.Y. Huang. 2006. Elemental composition and geochemical characteristics of iron-manganese nodules in main soils of China. Pedosphere 16:72–81. doi:10.1016/S1002-0160(06)60028-3

Timofeeva, Ya.O. 2008. Accumulation and fractionation of trace elements in soil ferromanganese nodules of different size. Geochem. Int. 46:260–267. doi:10.1134/S0016702908030038

Timofeeva, Ya.O., and V.I. Golov. 2007. Sorption of heavy metals by iron–manganic nodules in soils of Primorskii region. Euras. Soil Sci. 40:1308–1315. doi:10.1134/S1064229307120071

Tokashiki, Y., T. Hentona, M. Shimo, and L.P. Vidhana Arachchi. 2003. Improvement of the successive selective dissolution procedure for the separation of birnessite, lithiophorite and goethite in soil manganese nodules. Soil Sci. Soc. Am. J. 67:837–843. doi:10.2136/sssaj2003.0837

Vodyanitskiy, Yu.N. 2005. Manganese oxides in soils. V.V. Dokuchaev Soil Sci. Inst. of RAAS Press, Moscow, Russia.

Vodyanitskii, Yu.N. 2010. The Role of iron in the fixation of heavy metals and metalloids in soils: A review of publications. Euras. Soil Sci. 43:519–532. doi:10.1134/S1064229310050054

Zhang, M., and A.D. Karathanasis. 1997. Characterization of iron manganese concretions in Kentucky Alfisols with perched water tables. Clays Clay Miner. 45:428–439. doi:10.1346/CCMN.1997.0450312